





21 storage capacity curve, was derived to investigate the response of DUH to soil moisture  
22 content in unsaturated areas. Thus, an improved distributed unit hydrograph, based on  
23 time-varying soil moisture content, was developed. The proposed DUH considered the  
24 impact of both the time-varying rainfall intensity and soil moisture content on flow  
25 velocity, assuming the watershed to be not in equilibrium but varying with soil moisture.  
26 The Qin River basin and Longhu River basin were selected as two case studies, and the  
27 synthetic unit hydrograph (SUH), time-varying distributed unit hydrograph (TDUH)  
28 and the current DUH methods were compared with the proposed method. The influence  
29 of time-varying soil moisture content on the flow velocity and flow routing was  
30 evaluated. Results showed that the proposed method performed the best among the four  
31 methods. The shape and duration of the unit hydrograph can be mainly related to the  
32 soil moisture content at the initial stage of a rainstorm. When the watershed is  
33 approximately saturated, the grid flow velocity is mainly dominated by excess rainfall.  
34 **Keywords:** Time-varying distributed unit hydrograph, Runoff routing, Flow velocity,  
35 Soil moisture content, Excess rainfall

## 36 1. Introduction

37 Flood is a natural disaster with occurring suddenly and causing serious harm  
38 (Jongman et al., 2014; Alfieri et al., 2015; Munich, 2017). Global flood losses account  
39 for about 40% of the total losses of all kinds of natural disasters. Accurate flood  
40 forecasts can provide a decision-making basis for reservoir operation, flood control,



41 and optimal allocation of water resources, which, in turn, plays a significant role in  
42 water resources management, development and utilization, and economic growth and  
43 reconstruction.

44 Flow routing is an important component in a hydrological model, whose accuracy  
45 directly affects flow forecasting. The Unit Hydrograph (UH), proposed by Sherman  
46 (1932), is one of the methods most widely used in the development of flood prediction  
47 and warning systems for gauged basins with observed rainfall–runoff data (Singh et al.,  
48 2014). The UH, which is a surface runoff hydrograph resulting from one unit of rainfall  
49 excess uniformly distributed spatially and temporally over the watershed for the  
50 specified rainfall excess duration (Chow 1964), can be categorized into 4 major types  
51 (Singh, 1988), including traditional, probability, conceptual, and geomorphologic  
52 methods (Bhuyan et.al. 2015).

53 The traditional methods establish the relationships between parameters used to  
54 describe the UH (e.g. peak flow, time to peak and time base) and parameters used to  
55 describe the basin. Snyder (1938), Mockus (1957) and U.S. Soil Conservation Service  
56 (SCS) (2002) proposed some traditional methods, which are still used. The  
57 disadvantages of these methods are that they do not yield adequately satisfactory results,  
58 and their application to practical engineering problems is tedious and cumbersome  
59 (Nigussie et al., 2016).

60 Since most UHs have steeper rising limbs than their receding sides, which can be  
61 characterized by probability distribution functions (PDFs). Due to their similarity in the



62 shape of statistical distributions, many PDFs were used for the derivation of UHs. The  
63 difficulties of these methods are that the distribution functions are diverse, and the  
64 parameters depend on numerous hydrological data (Bhuyan et al., 2015).

65 Conceptual methods are another technique for deriving UHs. Nash (1957)  
66 proposed a conceptual model characterized as a succession of  $n$  linear reservoirs  
67 connected in series with the same storage coefficient  $K$  for the derivation of the  
68 instantaneous unit hydrograph (IUH). Dooge (1959) proposed a generalized IUH based  
69 on linear reservoirs, linear channels, and time-area concentration diagram. Bhunya et  
70 al. (2005) and Singh et al. (2007) represented a hybrid and extended hybrid model based  
71 on the linear reservoir model. Singh (2015) proposed a new simple two-parameter IUH  
72 with conceptual and physical justification. Khaleghi et al. (2018) suggested a new  
73 conceptual model, namely, the inter-connected linear reservoir model (ICLRM).  
74 However, the conceptual model neglects the impact of uneven spatial distribution of  
75 the basin's underlying surface on the UHs.

76 Using the time-area method developed by Clark (1945), Rodriguez-Iturbe (1979)  
77 proposed a geomorphologic instantaneous unit hydrograph (GIUH) method, which  
78 couples the hydrologic characteristics of a catchment with geomorphologic parameters  
79 (Kumar et al., 2007). In this method, the IUH corresponds to the probability density  
80 function of travel times from the locations of runoff production to the watershed outlet  
81 (Gupta et al., 1980; Singh, 1988). With the development of digital elevation models  
82 (DEMs) and geographic information system (GIS) technology, the formulation of width



83 function-based geomorphological IUH methods are available, the rigidity of which is  
84 reflected in its incapacity to account properly (i.e. to respect the geometry) for the  
85 distribution of rainfall (Rigon et al., 2016).

86 The UH method assumes some hypotheses (i.e. linear, time invariant, spatially  
87 homogeneous rainfall) in the application. Contrary to the linear assumption, basins have  
88 been shown to exhibit nonlinearity in the transformation of excess rainfall to stormflow  
89 (Bunster et al., 2019). Of course, this is an accepted compromise in challenging  
90 hydrological studies over the past few decades, especially for ungauged basins.  
91 Minshall (1960) showed that different rainfall intensities significantly corresponded to  
92 different UHs for a small watershed. Rodríguez-Iturbe et al. (1982) extended the GIUH  
93 to the geomorphoclimatic IUH (GcIUH) to cope with this nonlinearity by incorporating  
94 excess rainfall intensity in the determination of the IUH. Lee et al. (2008) proposed a  
95 variable Kinematic wave GIUH corresponding to time-varying rainfall intensity for the  
96 calculation of runoff concentration, which warrants consideration for rainfall-runoff  
97 modelling in ungauged catchments that are influenced by high intensity rainfall. Du et  
98 al. (2009) proposed a GIS based routing approach to simulate storm runoff with the  
99 consideration of spatial and temporal variability of runoff generation and flow routing  
100 through hillslope and river network. IA similar work was done by Muzik (1996),  
101 Gironás et al. (2009), and Bunster et al. (2019).

102 It is difficult for the traditional, probability, conceptual, and geomorphologic  
103 methods to fully consider the geomorphic characteristics of the watershed while



104 incorporating the nonlinearity of rainfall-runoff process (e.g. time-varying rainfall  
105 intensities). Thus, the spatially distributed unit hydrograph (DUH) method attracted  
106 much attention. The of DUH conceptualizes that the unit hydrograph can be derived  
107 from the time-area curve of a watershed by the S-curve method (Muzik, 1996). The  
108 DUH can be essentially classified as a type of geomorphoclimatic unit hydrograph,  
109 since its derivation depends on watershed geomorphology, rainfall, and flow hydraulics  
110 (Du et al., 2009). The spatially distributed flow celerity and temporally varying excess  
111 rainfall intensities can be considered in DUH (Bunster et al., 2019).

112 In the DUH method, the travel time of each grid cell can be calculated by dividing  
113 the travel distance of a cell to the next cell by the velocity of flow generated in that cell  
114 (Paul et al., 2018). The travel time is then summed along the flow path to obtain the  
115 total travel time from each cell to the outlet. The DUH is thus derived using the  
116 distribution of travel time from all grid cells in a watershed (Bunster et al., 2019). Some  
117 DUH methods assumed a time-invariant travel time field and ignored the dependence  
118 of travel time on excess rainfall intensity (Melesse & Graham, 2004; Noto and La  
119 Loggia, 2007; Gibbs et al., 2010), while others suggested various UHs corresponding  
120 to different storm events, namely time-varying distributed unit hydrograph (TDUH)  
121 (Martinez et al., 2002; Sarangi et al., 2007; Du et al., 2009). Compared to the fully  
122 distributed methods based on the momentum equation, the DUH method is a more  
123 efficient method that allows for the use of distributed terrain information in an  
124 ungauged region. The DUH methods better account for the spatial information of



125 watershed and time-varying rainfall-runoff process than do the traditional methods. The  
126 DUH also has been developed as an alternative method to semi-distributed and fully  
127 distributed methods for rainfall-runoff modelling (Bunster et al., 2019).

128 Besides excess rainfall intensity, researchers have also focused on the upstream  
129 contributions to the travel time estimation in the time-varying DUH method. For  
130 instance, Maidment et al. (1996) defined the velocity in the cell as a function of the  
131 contributing area to take into account the velocity increase observed downstream in  
132 river systems (Gironás et al., 2009). Gad (2014) applied a grid-based technique  
133 implementing the stream power formulation to relate flow velocity to the hydrologic  
134 parameters of the upstream watershed area through a simple parametric approach.  
135 Similar work has been done by Saghafian and Julien (1995), Bhattacharya et al. (2012)  
136 and Chinh et al. (2013). An important drawback of this method is the assumption that  
137 the watershed is near global equilibrium. Bunster et al. (2019) developed a spatially  
138 time-varying DUH model that accounts for dynamic upstream contributions and  
139 characterized the temporal behavior of upstream contributions and its impact on travel  
140 times in the basin. However, this time-varying DUH also assumed that equilibrium in  
141 each individual grid cell was reached before the end of the rainfall excess pulse. When  
142 there accrues continuous excess-rainfall in a watershed, the soil moisture content and  
143 surface runoff increase, and the infiltration rate decreases, leading to an acceleration of  
144 flow routing velocity, until the entire basin is saturated and the routing velocity reach  
145 its maximum. This assumption of equilibrium globally or in grid cells yields slower



146 travel times, shorter times to peak, and higher peak discharges. However, these  
147 approximations neglect the impact of dynamic changes of soil moisture exchange and  
148 water storage in unsaturated regions.

149 The objective of this study is therefore to propose a time varying distributed unit  
150 hydrograph method for runoff routing that accounts for dynamic rainfall intensity and  
151 soil moisture content based on the existing Xinanjiang (XAJ) model. The main  
152 contributions of the present study are as follows. First, a soil moisture content  
153 proportional factor in the unsaturated area was identified and expressed based on the  
154 Pareto distribution function. Second, the travel time expression function based on the  
155 kinematic wave theory was modified by considering the soil moisture content  
156 proportional factor. Besides rainfall intensity, the influence of time-varying soil  
157 moisture storage on flow velocity in the watershed was considered, where runoff  
158 generation is dominated by saturation-excess mode. Finally, the Qin River basin and  
159 Longhu River basin in the Guangdong Province, China, were selected as two case  
160 studies. The flow forecast method mainly consisted of the calculation of excess rainfall  
161 and the derivation of DUH. A new routing method was developed to incorporate the  
162 behavior of dynamic changes of soil moisture content and rainfall intensity, and the  
163 XAJ model was adopted to calculate the excess rainfall. The SUH, DUH and TDUH  
164 methods were compared with the proposed method, and sensitivity analysis of  
165 parameters was conducted.

## 166 2. Improvement of flow routing method





167 *2.1 Calculation of flow velocity considering time-varying soil moisture*  
168 *content*

169 The DUH relies on the computation of travel time over a basin. Grimaldi et al.  
170 (2010) found that the Soil Conservation Service (SCS) formula, given by Eq. (1), can  
171 be used to adequately define the basin flow time. This formula was also used by NRCS  
172 (1997) and Grimaldi et al. (2012), but this formula is time invariant and the time-  
173 varying rainfall intensity should be considered, which is given by Eq. (2). Wong (1995),  
174 Muzik (1996), Bedient and Huber (2002), Gironas et al. (2009), Du et al. (2009) and  
175 Kong et al. (2019) used this formula.

176 
$$V = k \cdot S^{\frac{1}{2}} \quad (1)$$

177 
$$V = k \cdot S^{\frac{1}{2}} \cdot \left( \frac{I_t}{I_c} \right)^{\frac{2}{5}} \quad (2)$$

178 where  $V$  (m/s) is the flow velocity;  $k$  (m/s) is land use or flow type coefficient;  $S$  (m/m)  
179 is the slope of the grid cell;  $I_t$  (mm/h) represents the excess rainfall intensity at time  $t$ ;  
180 and  $I_c$  (mm/h) represents the reference excess rainfall intensity of the basin.

181 These formulas assume that equilibrium in individual grid cell can be reached  
182 before the end of the rainfall excess (Bunster et al., 2019), which leads to larger flow  
183 velocity, shorter travel time, and higher peak discharge. Actually, the hillslope flow  
184 velocity in each grid is related to soil moisture content. Fast subsurface velocities and  
185 quick runoff responses to precipitation have been observed on many hillslopes  
186 (Hutchinson & Moore, 2000; Peters et al., 1995; Tani, 1997). The exact mechanisms



187 that cause water to move through the preferential flow path network are not well  
188 quantified, but it is often assumed that saturated soil provides the connection between  
189 preferential features (Sidle et al., 2001; Steenhuis et al., 1988). Many studies have also  
190 shown that antecedent moisture condition, precipitation intensity, precipitation amount,  
191 topography and so on play a significant role in this phenomenon (Sidle et al., 2000;  
192 Tsuboyama et al., 1994; Anderson et al., 2009).

193 To that end, a soil moisture factor  $\theta_t$  was introduced to characterize the soil  
194 moisture content in unsaturated areas. Because the flow velocity will reach its  
195 maximum value when the entire basin is saturated, this new factor ( $\theta_t$ ) was added to  
196 the current time-varying flow velocity formula as

$$197 \quad V = k \cdot S^{\frac{1}{2}} \cdot \left( \frac{I_t}{I_c} \right)^{\frac{2}{5}} \cdot (\theta_t)^\gamma \quad (3)$$

198 where  $\theta_t$  (unitless) represents the state of the soil moisture content of unsaturated  
199 areas at time  $t$ ; and  $\gamma$  (unitless) is an exponent smaller than unity, which represents the  
200 nonlinear relationship between soil moisture content and flow velocity.

201 The factor  $\theta_t$  was defined as the ratio of  $w_t$  and  $w_{\max,t}$ , which is expressed by

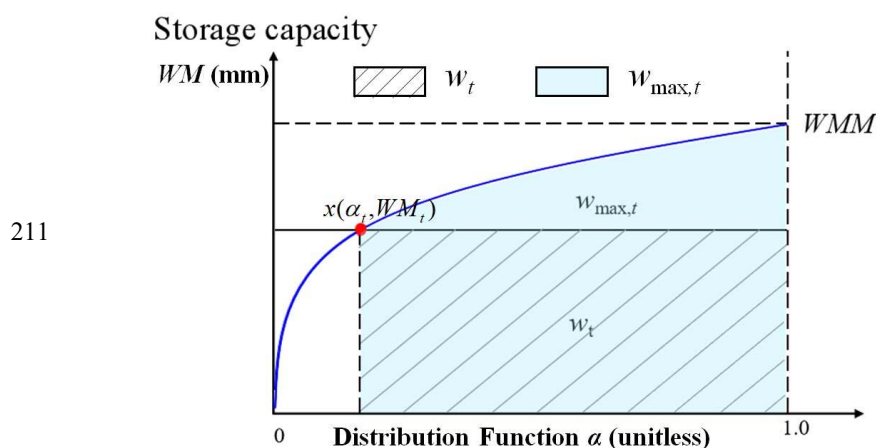
$$202 \quad \theta_t = \frac{w_t}{w_{\max,t}} \quad (4)$$

203 where  $w_t$  (mm) represents the mean tension water storage of the unsaturated region; and  
204  $w_{\max,t}$  (mm) represents the maximum tension water storage of the unsaturated region at  
205 time  $t$ .

206 Specifically,  $w_t$  and  $w_{\max,t}$  were calculated based on the Pareto distribution function



207 in this study. The Pareto distribution function has mostly been used to express the  
 208 spatial variability of soil moisture capacity (Moore, 1985), which is shown in Fig. 1. As  
 209 shown in the figure, the area below this curve represents the mean tension water  
 210 capacity of the entire basin.



212 **Figure 1.** Watershed storage capacity curve

213 For the tension water storage capacity curve, the specific formula is given by

$$214 \quad \alpha = 1 - \left( 1 - \frac{WM}{WMM} \right)^b \quad (5)$$

215 where  $\alpha$  (unitless) represents the proportion of the basin area where the tension water  
 216 capacity is less than or equal to the value of the ordinate  $WM$  (mm). The tension water  
 217 capacity at a point,  $WM$ , varies from 0 to a maximum  $WMM$  (mm) according to Eq. (5).

218 Actually, the soil moisture content in a basin varies with time. The state of the  
 219 catchment at any time  $t$  can be represented by a point  $x(\alpha_t, WM_t)$  on the curved line  
 220 of Fig. 1 (Zhao, 1992). The area to the right and below the point  $x$  is proportional to the  
 221 areal mean tension water storage (not capacity). Thus,  $WM_t$ , the ordinate of the point



222  $x$ , represents the tension water storage capacity in the basin at time  $t$ ;  $w_t$  (mm) can be  
 223 assumed to represent the mean tension water storage of the unsaturated region, and  
 224  $w_{\max,t}$  (mm) represents the maximum tension water storage of the unsaturated region at  
 225 time  $t$ . Their expressions are given by

$$226 \quad \alpha_t = 1 - \left(1 - \frac{WM_t}{WMM}\right)^b \quad (6)$$

$$227 \quad w_t = (1 - \alpha_t) \cdot WM_t \quad (7)$$

$$228 \quad w_{\max,t} = \int_{\alpha_t}^1 WMM \left[1 - (1 - \alpha)^{\frac{1}{b}}\right] d\alpha \quad (8)$$

229 Combining Eqs. (4), (7), (8), the soil moisture content can be written as

$$230 \quad \theta_t = \frac{w_t}{w_{\max,t}} = \frac{(1 - \alpha_t) \cdot WM_t}{\int_{\alpha_t}^1 WMM \left[1 - (1 - \alpha)^{\frac{1}{b}}\right] d\alpha} \quad (9)$$

231 Substituting Eq. (6) into Eq. (9),

$$232 \quad \theta_t = \frac{(1 - \alpha_t) \cdot WM_t}{WMM \left[1 - \alpha_t - \frac{b}{b+1} (1 - \alpha_t)^{1+\frac{1}{b}}\right]} = \frac{(b+1)WM_t}{WMM + bWM_t} \quad (10)$$

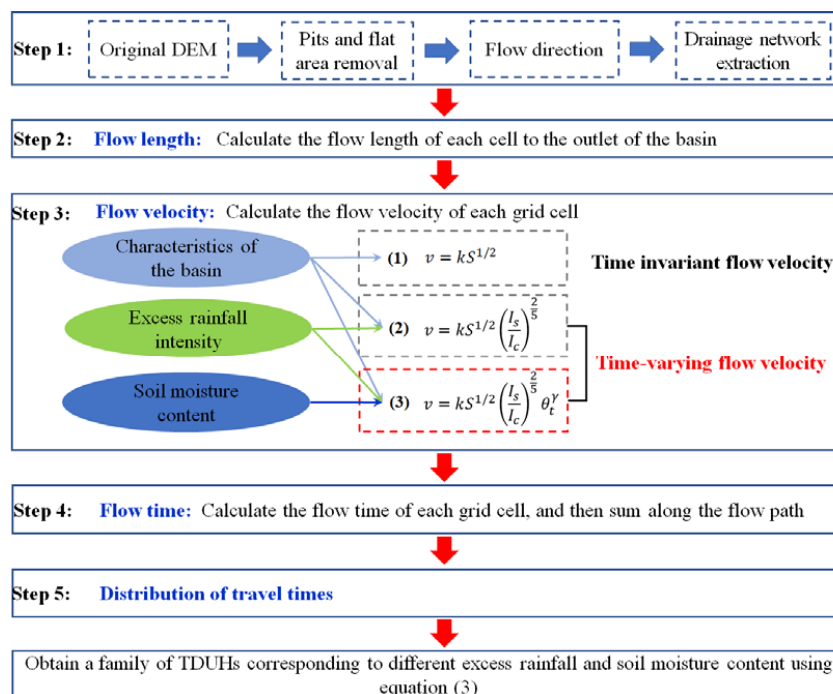
233 It can be seen from Eq. (10) that as rainfall continues, the soil moisture content in  
 234 the unsaturated area continues to increase, whereas the non-runoff area continues to  
 235 decrease. The ranges of  $\theta_t$  is (0, 1], and with the gradual increase of soil moisture,  $\theta_t$   
 236 tends to 1.



237 *2.2 Calculation of runoff routing based on DUH*

238 The GIS-derived DUH method was employed for runoff routing calculations,  
239 which allowed the velocity to be calculated on a grid cell basis over the watershed. The  
240 DUH routing method is a semi-analytical form of the width function-based IUH  
241 enumerated by Rigon et al. (2016). The DUH has been used for small ungauged basins.  
242 To remove the linearity assumption, fully distributed models use routing methods which  
243 are usually computationally intensive because they solve the St. Venant equations  
244 (Bunster et al., 2019), so they are usually limited to small basins. Therefore, the DUH  
245 method is an alternative method that allows the use of distributed information in a much  
246 more efficient manner, and we apply it to different sizes of watersheds.

247 The core of the DUH method is to equate the probability density function of time  
248 at which the rainfall flows to the outlet of the basin to the instantaneous unit hydrograph,  
249 in which the time-area relationship is derived using the velocity field with spatial  
250 distribution characteristics. The traditional DUH method can route the time-variant  
251 spatially distributed rainfall to the watershed outlet, and such a method is a lumped  
252 linear model of watershed response (Grimaldi et al., 2010). The schematic diagram of  
253 the proposed DUH method is shown in Fig. 2.



254

255 **Figure 2.** Schematic diagram of the DUH method considering time-varying rainfall  
 256 intensity and soil moisture content, in which Eqs. (1), (2) and (3) are the time invariant  
 257 flow velocity, time-varying flow velocity considering excess rainfall intensity, and  
 258 time-varying flow velocity considering both excess rainfall intensity and soil moisture  
 259 content. The unit hydrograph derived from the three flow velocity equations correspond  
 260 to DUH, TDUH and the proposed method respectively.

261 The processes of the DUH method are summarized as follows.

262 1) The drainage network using advanced DEM pre-processing techniques is  
 263 identified. More details can be found in Grimaldi et al. (2012).

264 2) Estimate the flow path, which is measured for each grid cell along the flow  
 265 directions to the outlet of basins.



266 3) Calculate the flow velocity based on the characteristics of the watershed and  
267 the spatial–temporal distribution characteristics of rainfall. Several flow velocity  
268 formulas are commonly used for deriving the spatially distributed unit hydrograph, such  
269 as the Manning’ formula (Chow et al., 1988), SCS formula (Haan et al., 1994), Darcy-  
270 Weisbach formula (Katz et al., 1995), and Maidment et al. (1996) uniform flow  
271 equation.

272 4) To compute the total travel time  $\tau_i$  of flow from each cell  $i$  to the outlet, we  
273 added travel times along the  $R_i$  cells belonging to the flow path that starts at that cell,  
274 given by Eq. (11) (Muzik, 1996). The travel time for each grid cell can be calculated  
275 using Eq. (12):

$$276 \quad \tau_i = \sum_{i \in R_i} \Delta \tau_i \quad (11)$$

$$277 \quad \Delta \tau_i = \frac{L_i}{V} \quad \text{or} \quad \Delta \tau_i = \frac{\sqrt{2}L_i}{V} \quad (12)$$

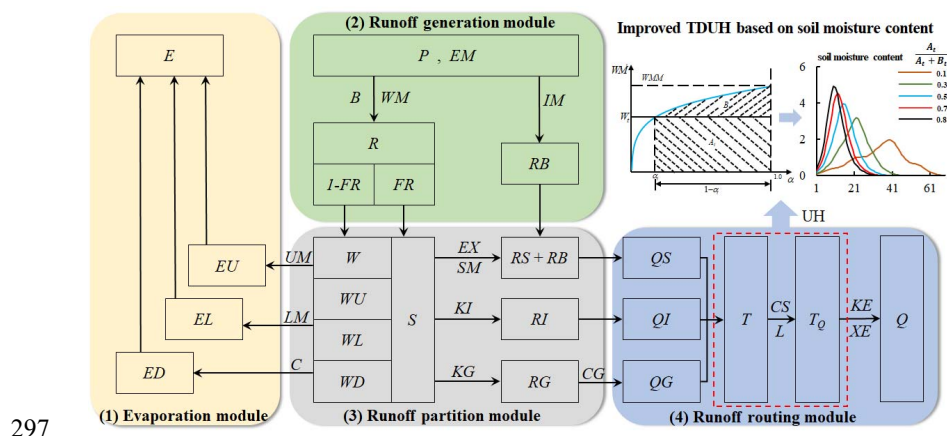
278 where  $\Delta \tau_i$  is the retention time in grid cell  $i$ ;  $\tau_i$  is the total travel time along the flow  
279 path in grid cell  $i$ ;  $L_i$  is the grid cell size; travel length in a specific grid cell is the cell  
280 size  $L_i$  when the rasterized flow is flowing along the edges of the grid, whereas travel  
281 length is  $\sqrt{2}L_i$  when it is flowing diagonally.

282 5) Develop a cumulative travel time map of the watershed based on cell by cell  
283 estimates for hillslope velocities. The cumulative travel time map is further divided into  
284 isochrones, which can be used to generate a time-area curve and the resulting unit  
285 hydrograph (Kilgore, 1997).



### 286 3. Calculation of runoff generation

287 The Xinanjiang (XAJ) model was used for the calculation of excess rainfall in this  
 288 study. It is a conceptual hydrologic model proposed by Zhao et al. (1980) for flood  
 289 forecasts in the Xinan River basin. The XAJ model has been widely used in humid and  
 290 semi-humid watersheds all over the world (Zhao, 1992). It mainly consists of four  
 291 modules, namely evapotranspiration module, runoff generation module, runoff partition  
 292 module and runoff routing module (Zhou et al., 2019). Usually, a large watershed is  
 293 divided into several sub-basins to capture the spatial variability of underlying surface,  
 294 precipitation, and evaporation. In each sub-basin, the inputs of the XAJ model are the  
 295 average areal rainfall as well as evaporation, and the output is streamflow. The  
 296 schematic diagram of the XAJ model is shown in Fig. 3.



297

298 **Figure 3.** Schematic diagram of the XAJ model

299 First, for the evapotranspiration module, the soil profile of each sub-basin is  
 300 divided into three layers, the upper, lower and deeper layers, and only when the layer  
 301 above it has exhausted water, evaporation from the next layer occurs. Second, as for





302 runoff generation in the XAJ model, a catchment is divided into two parts by the  
303 percentage of impervious and saturated areas, namely permeable and impervious areas,  
304 respectively. Since the soil moisture deficit is heterogeneous, runoff distribution is  
305 usually nonuniform across the basin. Thus, a storage capacity curve was adopted by the  
306 XAJ model to accommodate the nonuniformity of soil moisture deficit or the tension  
307 water capacity distribution. Third, the runoff partition in the XAJ model divides the  
308 total runoff into three components by a free reservoir, which consists of surface runoff  
309 (RS), interflow runoff (RI), and groundwater runoff (RG). More details can be found in  
310 (Zhao et al., 1980). Finally, the SUH, DUH, TDUH and the proposed method were used  
311 to calculate flow routing, respectively. The Maskingen method was employed to  
312 produce streamflow from each sub-basin to the outlet of the entire catchment.

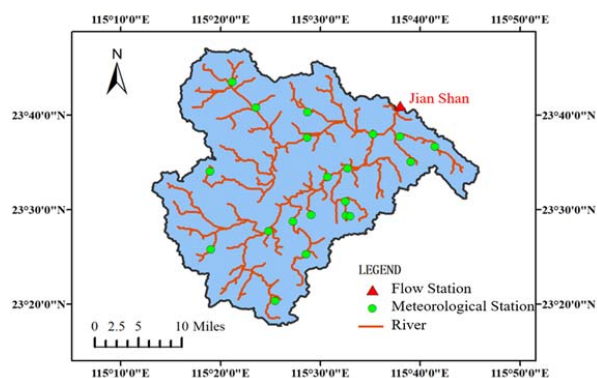
#### 313 **4 Study area and data**

314 The Qin River basin and Longhu River basin were selected as two case study  
315 watersheds. One is a large watershed, and the other is a small watershed. The  
316 applicability of the proposed method to different size watersheds was verified, and  
317 parameter sensitivity analysis was done to evaluate the performance of the proposed  
318 method.

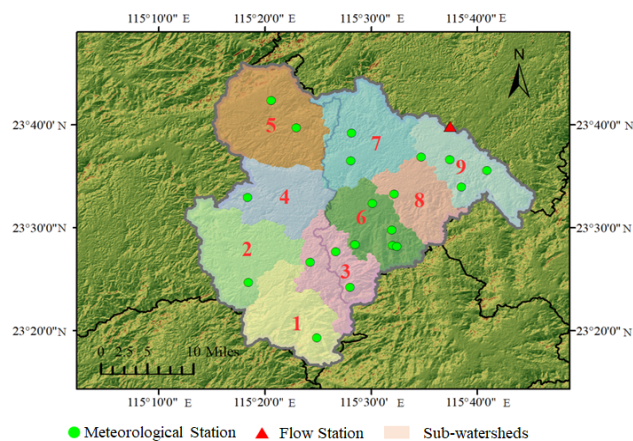
319 The Qin River is a tributary of the Mei River, which originates from Guangdong  
320 Province, China. The river is 91 km long with a basin area of 1578 km<sup>2</sup>. The mean slope  
321 of the basin is 1.1‰. There are 21 meteorological stations and 1 flow station (the



322 Jianshan Station) in this area, as shown in Fig. 4. Using the DEM data of the Qin River  
323 basin, the whole basin was divided into 9 sub-basins, based on the natural water system,  
324 namely sub-basins 1-9 from upstream to downstream as shown in Fig. 5. Details of each  
325 sub-basin are given in Table 1.



326  
327 **Figure 4.** Distribution diagram of meteorological stations and flow stations in the Qin  
328 River basin



329  
330 **Figure 5.** Sub-basins of the Qin River basin (*Note.* The satellite images for  
331 the study area are available at <http://www.gscloud.cn>)

332



333

334

**Table 1.** Information on sub-basins

Sub-basins	Drainage area/km <sup>2</sup>	Number of grids	Average slope
Sub-basin 1	175.64	176	13.29
Sub-basin 2	195.86	197	9.27
Sub-basin 3	154.97	156	12.50
Sub-basin 4	153.08	151	9.57
Sub-basin 5	147.79	147	12.49
Sub-basin 6	249.36	253	11.74
Sub-basin 7	213.34	211	10.56
Sub-basin 8	122.28	129	10.77
Sub-basin 9	166.51	161	9.74

335 The Longhu River basin is a small watershed, which has a drainage area of 102.7  
336 km<sup>2</sup>, located in the Guangdong Province, China. The length of the River is 17.4 km.

337 The rainfall and evaporation data from meteorological stations was collected from  
338 1959 to 2018. The simultaneous hourly runoff data for the Jianshan Station and Longhu  
339 Station was collected as well. The antecedent precipitation was calculated, based on the  
340 daily recession coefficient of water storage in the basin.

## 341 **5. Results and discussion**

### 342 *5.1 Calibration of parameters*

#### 343 *5.1.1 Model calibration*

344 The SCE-UA (Shuffled Complex Evolution Algorithm) method, developed by the  
345 University of Arizona in 1992 (Duan et al., 1992), is suitable for nonlinear, high  
346 dimension optimization problems. The method has been widely used for the calibration  
347 of hydrological models (Vrugt et al., 2006; Beskow et al., 2011; Zhou et al., 2018).



348 Hence, the SCE-UA method was used to optimize the parameters of XAJ model in this  
 349 study.

350 The Nash-Sutcliffe efficiency ( $E_{NS}$ ) (Nash and Sutcliffe, 1970), the Kling-Gupta  
 351 efficiency ( $E_{KG}$ ) (Gupta et al., 2009), and the root-mean-squared error to standard  
 352 deviation ratio ( $R_{SR}$ ) were chosen as criteria. Moreover, the new aggregated objective  
 353 function (Brunner et al., 2021) targeted at optimizing flow characteristics was  
 354 composed of these three metrics, in which  $E_{KG}$  focuses on high flows (Mizukami et al.,  
 355 2019),  $\log(E_{NS})$  emphasizes low flows, and  $R_{SR}$  quantifies volume errors. Three metrics  
 356 and the aggregated objective function are expressed by

$$357 \quad E_{NS} = 1 - \frac{\sum_{t=1}^T |Q_s^t - Q_o^t|}{\sum_{t=1}^T |Q_o^t - \bar{Q}_o|} \quad (13)$$

$$358 \quad E_{KG} = 1 - \sqrt{(r-1)^2 + \left(\frac{\sigma_s}{\sigma_o} - 1\right)^2 + \left(\frac{\mu_s}{\mu_o} - 1\right)^2} \quad (14)$$

$$359 \quad R_{SR} = \sqrt{\frac{\sum_{t=1}^T (Q_o^t - Q_s^t)^2}{\sum_{t=1}^T (Q_o^t - \bar{Q}_o)^2}} \quad (15)$$

$$360 \quad M = 0.5 \times (1 - E_{NS}) + 0.25 \times (1 - E_{KG}) + 0.15 \times (1 - \log(E_{NS})) + 0.1 \times R_{SR} \quad (16)$$

361 where  $Q_o^t$  is observed discharge at time  $t$ ;  $Q_s^t$  is simulated discharge at time  $t$ ;  $\bar{Q}_o$   
 362 is the mean of observed discharge;  $T$  is duration of the flood event;  $r$  is correlation  
 363 coefficient between the observed and simulated flood;  $\sigma_s$  and  $\sigma_o$  are the standard  
 364 deviation values for the simulated and observed responses, respectively; and  $\mu_s$  and  $\mu_o$   
 365 are the corresponding mean values.



366 *5.1.2 Calibrated parameters of runoff generation using the XAJ Model*

367         Since the Qin River basin and Longhu River basin are in the humid area of  
368 southern China, the saturation-excess method with three-source runoff separation of the  
369 XAJ model was adopted to calculate the excess rainfall. A total of 64 isolated storms  
370 with the observed runoff responses from 1959 to 2018 were selected to calibrate and  
371 verify the model, of which 35 events were collected from the Qin River basin and 29  
372 from the Longhu River basin. 25 and 23 flow events were used for model calibration in  
373 the Qin and Longhu River basins respectively, and 10 and 6 flow events were used for  
374 model validation in the two basins. The initial condition of the XAJ model was  
375 considered by calculating the antecedent precipitation index before each flow event  
376 (Linsley et al. 1949).

377         In addition, the parameters of the XAJ model and the proposed distributed unit  
378 hydrograph were calibrated separately. Since the objective of this study is to propose a  
379 new flow routing method, the runoff producing model with its parameters were not  
380 changed in order to discuss the performance of the flow routing models. The synthetic  
381 unit hydrograph, derived by historical rainfall-runoff data, was used for flow routing in  
382 the process of model calibration. The time interval was 1 hour. The flow peak, flow  
383 volume, and the occurrence time of flow peak are three main basic elements for  
384 describing the flow hydrograph, and Eq. (16) was used as the aggregated objective  
385 function. The average Nash-Sutcliffe efficiency, relative flood peak error, and peak  
386 occurrence time error obtained in the calibration period of the XAJ model are 0.84,



387 10.4%, and 4.96 hours respectively for the Qin River basin. Accordingly, for the  
 388 Longhu River basin, it is 0.86, 8.81%, and 2.75 hours respectively, indicating a good  
 389 performance of the XAJ model. Detailed information on the calibrated parameters of  
 390 the XAJ model is shown in Table 2.

391 **Table 2.** Calibrated parameters of the XAJ model

Parameters	Physical meaning	The Qin River	The Longhu River	Unit
<i>UM</i>	Averaged soil moisture storage capacity of the upper layer	20.05	8.24	mm
<i>LM</i>	Averaged soil moisture storage capacity of the lower layer	74.42	72.98	mm
<i>DM</i>	Averaged soil moisture storage capacity of the deep layer	26.54	22.30	mm
<i>B</i>	Exponential of distribution of tension water capacity	0.25	0.12	-
<i>IM</i>	Ratio of impervious to total areas in the catchment	0.01	0.01	-
<i>K</i>	Ratio of potential evapotranspiration to pan evaporation	0.85	0.89	-
<i>C</i>	Evapotranspiration coefficient of the deeper layer	0.15	0.12	-
<i>SM</i>	Free water capacity of the surface layer	45.32	50.23	mm
<i>EX</i>	Exponent of the free water capacity curve influencing the development of the saturated area	1.50	1.50	-
<i>KI</i>	Outflow coefficient of free water storage to interflow	0.38	0.13	-
<i>KG</i>	Outflow coefficient of free water storage to groundwater	0.26	0.65	-
<i>CI</i>	Recession constant of the lower interflow storage	0.85	0.83	-
<i>CG</i>	Recession constant of the ground water storage	0.99	0.99	-
<i>CS</i>	Recession constant in the lag and rout method for routing through the channel system within each sub-basin	0.46	0.7	-
<i>KE</i>	Muskingum time constant for each sub-reach	22.80	3.5	-
<i>XE</i>	Muskingum weighting factor for each sub-reach	0.13	0.12	-

392

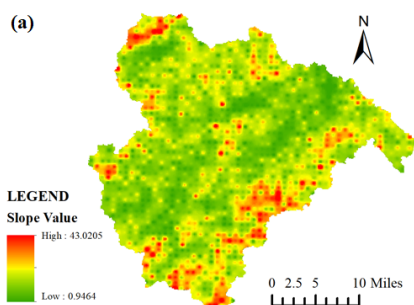


393 *5.1.3 Calibrated Parameters of the proposed flow routing method*

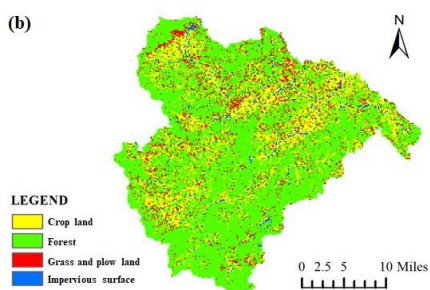
394 As mentioned in Section 2.2, the core of the DUH is the calculation of the grid  
395 flow velocity. As shown in Eq. (3), the parameters that need to be calibrated are  $K$ ,  $S$ ,  $I_c$   
396 and  $\gamma$ , in which  $I_c$  can be determined using hourly mean rainfall intensity and flow  
397 forecast of the target basin. For the Qin River basin,  $I_c$  was set at 20 mm/h, because the  
398 mean rainfall intensity of multiple flows was about 20mm/h, and this parameter was 10  
399 mm/h for the Longhu River basin. Additionally, parameter  $\gamma$  reflected the influence  
400 of soil moisture content in unsaturated regions on flow velocity. The smaller the  
401 parameter  $\gamma$  was, the smaller the influence of soil moisture content on the flow  
402 velocity was. When the value of  $\gamma$  was equal to 1, the flow velocity of grid cell was  
403 proportional to the soil moisture content factor  $\theta_i$ . The parameter  $\gamma$  of soil moisture  
404 content was determined to be 0.5 to reflect the influence of soil moisture content on the  
405 flow velocity for the two basins. Furthermore, sensitivity analysis for this parameter  
406 was conducted in Section 5.6. In order to get the grid cell slope  $S$ , the slope distribution  
407 of the study areas was obtained from the DEM data of the target basin. Fig. 6(a) plots  
408 the slope distribution of the Qin River basin. The parameter  $k$  is the velocity coefficient,  
409 which was determined, based on different underlying surface types or different flow  
410 states (Ajward & Muzik, 2000). The parameter  $k$  changes with different land types, and  
411 the  $k$  values used in this study are given in Table 3. The land types of the Qin River  
412 basin are shown in Fig. 6(b). Then the  $k$  values of each grid cell were determined by  
413 combining Fig. 6(b) and Table 3.



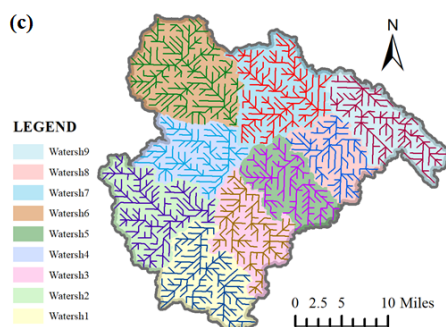
414



415



416



417 **Figure 6.** Slope, Land types and rasterized flow direction of the Qin River basin

418 (a) Slope distribution. (b) Land types. (c) Rasterized flow direction.

419 **Table 3.** Specific values of  $k$  for different vegetational types





Land type	Vegetational form	$k$ (m/s)
Crop land	Fallow	1.37
	Contour tillage	1.40
	Straight plough	2.77
Grass and plow land	Trample	0.30
	Lush	0.46
	Sparse	0.64
	Pasture	0.40
Forest	Dense	0.21
	Sparse	0.43
	Full of dead leaves	0.76
Impervious surface	\	6.22

420 The grid flow velocity was calculated by Eq. (3) with the above parameter values.  
421 Then, the flow travel time was determined by Eq. (11) and Eq. (12). It is noteworthy  
422 that the raster size of the Qin River nasin was divided into 1km×1km, and the rasterized  
423 flow direction of each sub-basin is shown in Fig. 6(c). For the Longhu River basin, the  
424 difference was that its cell size was divided into 30m×30m to evaluate the performance  
425 of the proposed method in this small watershed.

## 426 5.2 Calculation of the proposed time-varying DUH

427 After determining the parameters above, flow routing was calculated, based on the  
428 proposed DUH considering the time-varying soil moisture content. In order to improve  
429 the efficiency and effectiveness of the routing method, the rainfall intensity and soil  
430 moisture content parameters were discretized. Then, a simplified TDUH considering  
431 time-varying soil moisture content and TDUH were obtained in a certain range of



432 rainfall intensities or soil moisture contents; these ranges are presented in Tables 4 and  
 433 5. To evaluate the performance of the proposed method, the traditional SUH, DUH and  
 434 TDUH methods were used for comparison.

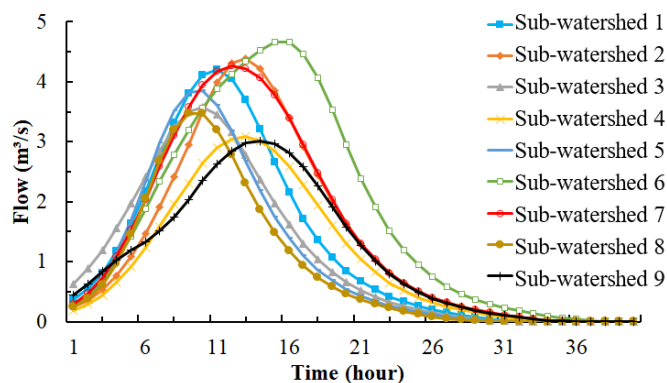
435 **Table 4.** The ratio of  $I_t$  to  $I_c$  of each period corresponds to the discrete rain intensity  $I_s$

$I_t / I_c$ (mm/h)	$0 < \frac{I_t}{I_c} \leq 0.5$	$0.5 < \frac{I_t}{I_c} \leq 1$	$1 < \frac{I_t}{I_c} \leq 1.5$	$\frac{I_t}{I_c} > 1.5$
Discrete $I_s$ (mm/h)	0.5	1	1.5	2

436 **Table 5.** The soil moisture content  $\theta_t$  of each period corresponds to the discrete soil  
 437 moisture content  $\theta_s$

Soil moisture content $\theta_t$	$0 < \theta_t \leq 0.2$	$0.2 < \theta_t \leq 0.4$	$0.4 < \theta_t \leq 0.6$	$0.6 < \theta_t \leq 0.8$	$\theta_t > 0.8$
Discrete soil moisture content $\theta_s$	0.1	0.3	0.5	0.7	0.85

438 The DUH without considering rainfall intensity and soil moisture was obtained  
 439 using Eq. (1). Results of the DUH for each sub-basin of the Qin River basin are shown  
 440 in Fig. 7. There is only one DUH for a specific sub-basin due to the simplification of  
 441 the underlying surface, such as slope and land covers. The differences among the DUHs  
 442 were mainly reflected in flow peaks and their occurrence times. It can be also seen from  
 443 Fig. 7 that the peak of DUHs in sub-basins 4 and 6 were significantly lower than in  
 444 others. The reason may be that the smaller mean slop values of sub-basins 4 and 6 lead  
 445 to lower flow velocity, resulting in lower peak of the DUH.



446

447

**Figure 7.** DUH for the Qin River basin

448

449

450

451

452

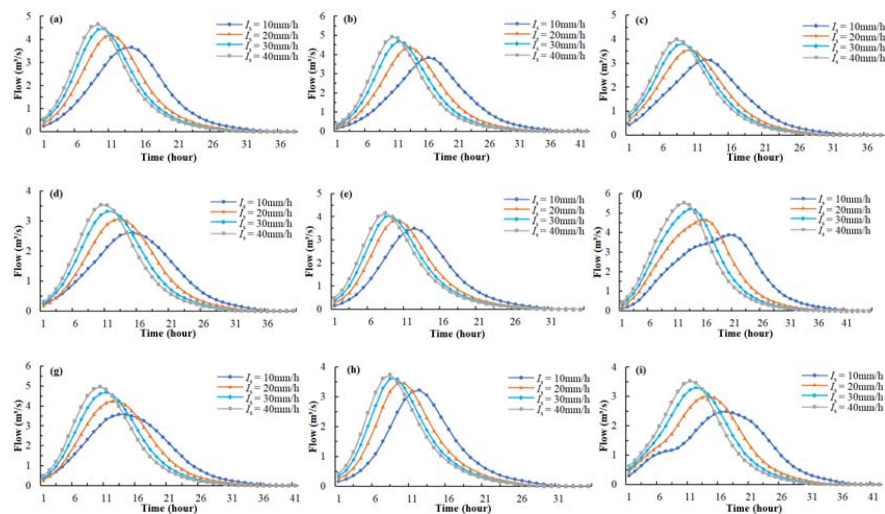
453

The TDUHs corresponding to different rainfall intensities of 9 sub-basins are shown in Fig. 8. It can be seen from Fig. 8 that different rainfall intensities corresponded to different TDUHs. The increased rainfall intensity led to higher peak and earlier peak occurrence time of the UH. This is because that a larger rainfall intensity caused a larger flow velocity according to Eq. (2). In the practical use of TDUH, the UHs need to be selected according to rainfall intensities.

454

455

456



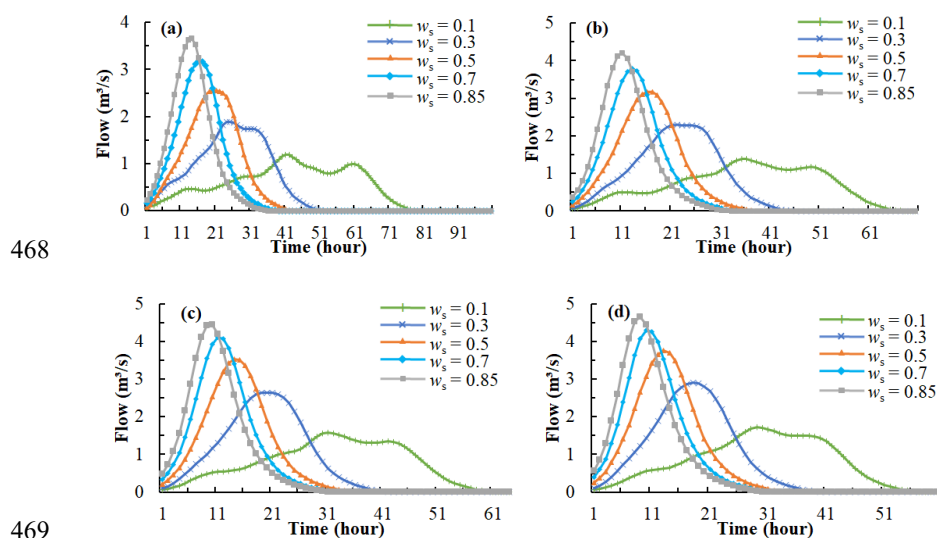
457

**Figure 8.** The TDUH for the Qin River basin. (a) Sub-basin 1. (b) Sub-basin 2. (c) Sub-



458 basin 3. (d) Sub-basin 4. (e) Sub-basin 5. (f) Sub-basin 6. (g) Sub-basin 7. (h) Sub-basin  
459 8. (i) Sub-basin 9.

460 The TDUH of each sub-basin was further divided according to the soil moisture  
461 content. The TDUHs considering soil moisture contents of sub-basin 1 are shown in  
462 Fig. 9. Obviously, under the same rainfall intensity, the soil moisture content was of  
463 great importance to the shape, peak value and duration of the TDUH. Specifically, when  
464 the proportion of soil moisture content  $\theta_i$  increased, the proposed method considering  
465 soil moisture content was accompanied by steeper rising limb, higher peak and shorter  
466 duration. After the whole basin was saturated, the TDUH considering the soil moisture  
467 content was the same as the TDUH.

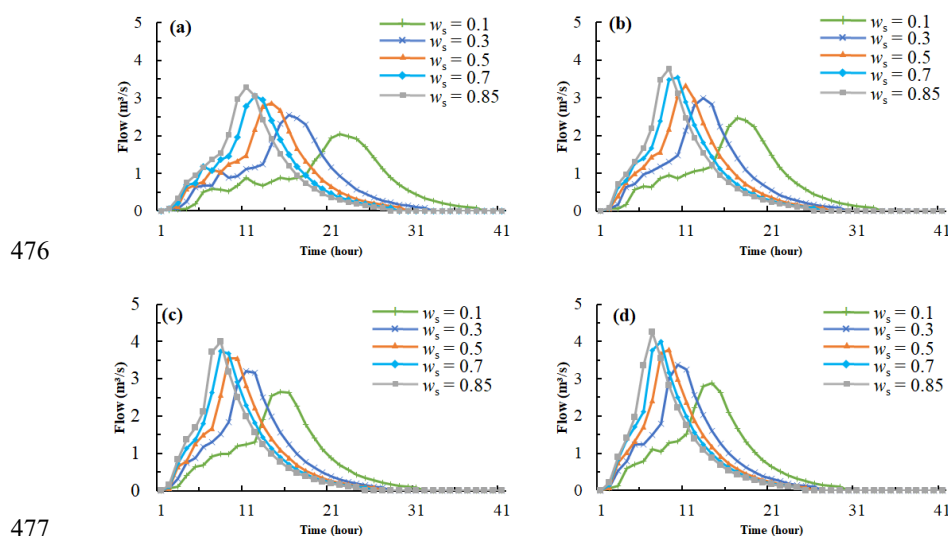


470 **Figure 9.** The TDUH considering soil moisture content for sub-basin 1 of the Qin  
471 River basin. (a)  $I_s = 0.5$ . (b)  $I_s = 1$ . (c)  $I_s = 1.5$ . (d)  $I_s = 2$ .

472 Similarly, the TDUHs considering the soil moisture content for the Longhu River



473 basin are shown in Fig. 10. The grey line in Fig. 10(b) is the DUH, where  $I_s$  is equal  
474 to 1 and  $w_s$  is 0.85. Four grey unit hydrographs in Fig. 10(a) to 10(d) make up the  
475 TDUH without considering the soil moisture content.



476  
477  
478 **Figure 10.** The TDUH considering soil moisture content for the Longhu River basin.  
479 (a)  $I_s = 0.5$ . (b)  $I_s = 1$ . (c)  $I_s = 1.5$ . (d)  $I_s = 2$ .

### 480 5.3 Comparison of flood routing methods

481 The runoff generation module of the XAJ model was used to calculate the excess  
482 rainfall, and the SUH, DUH, TDUH and improved TDUH considering soil moisture  
483 content were employed for flow routing calculations, respectively. Dozens of flow  
484 events were applied for model validation. Simulated results of the four methods for the  
485 Qin River basin are shown in Table 6. Three criteria were used for model performance  
486 evaluation, which included the Nash-Sutcliffe efficiency ( $E_{NS}$ ), the ratio between the



487 simulated and observed peak discharges ( $Q_p^s / Q_p^o$ ), and the error between simulated and  
 488 observed times to peak ( $|t_p^s - t_p^o|$ ). The ratio between simulated and observed peak  
 489 discharges of the proposed method ranged from 0.97 to 1.10. The average peak  
 490 occurrence time error of the proposed method was 1.4h, which was the smallest among  
 491 the four methods, and the mean  $E_{NS}$  coefficients of the ten flow events for validation  
 492 were above 0.8. Fig. 11 shows the flow hydrographs of the four routing methods for  
 493 part of the flow events (Event No. 20130720, 20130817, 20150709, 20160128,  
 494 20161021 and 20180916). It is demonstrated that the proposed method outperformed  
 495 the remaining three routing methods.

496 In addition, the forecast results of six flow events in the Longhu River basin using  
 497 the SUH, DUT, TDUH and the proposed method are presented in Table 7. Results of  
 498 the proposed method generally showed the best performance, which also verified the  
 499 proposed formula in the small watershed. In general, the proposed method did better  
 500 simulation in this watershed than in the Qin River basin.

501 **Table 6.** Comparison of four routing methods for the Qin River basin

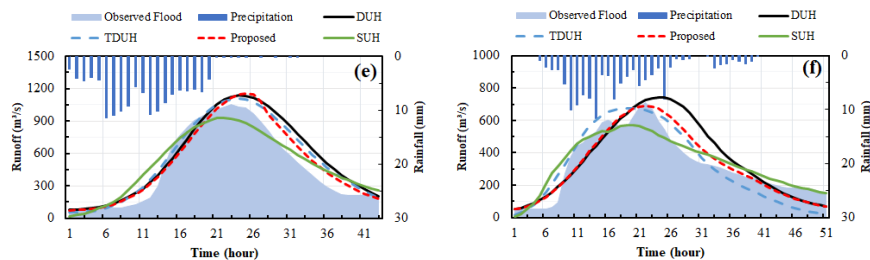
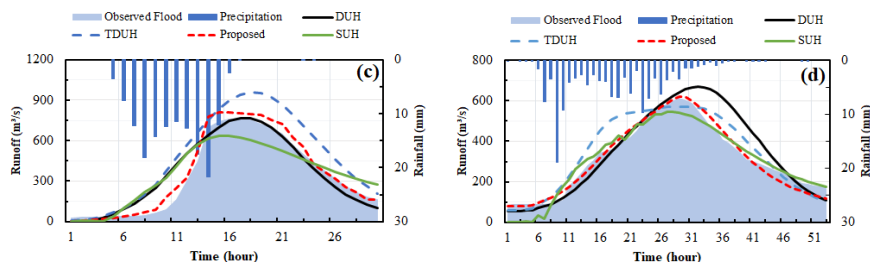
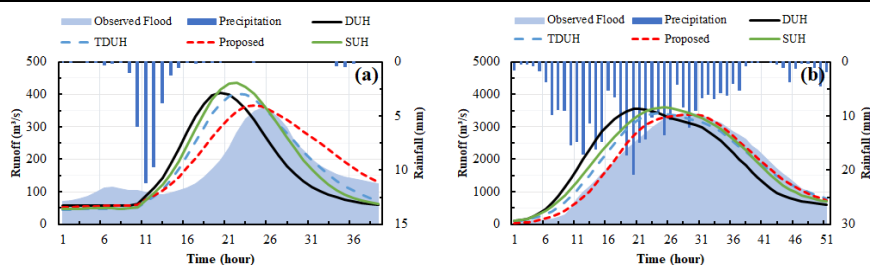
Event number	$(Q_p^s / Q_p^o) / ( t_p^s - t_p^o ) / (E_{NS})$			
	SUH	DUH	TDUH	Proposed
20130720	1.16/1/0.44	1.13/3/0.32	1.13/3/0.31	<b>1.02/1/0.64</b>
20130817	1.06/3/0.86	1.04/7/0.61	1.01/4/0.92	<b>0.99/1/0.98</b>
20130922	0.95/2/0.82	1.07/3/0.82	<b>1.04/2/0.87</b>	0.98/3/0.85
20150709	0.83/0/0.80	1.01/2/0.87	1.26/2/0.63	<b>1.07/1/0.97</b>
20160128	0.89/2/0.93	1.09/3/0.74	0.93/1/0.83	<b>1.01/0/0.97</b>
20160827	1.14/3/0.83	1.10/2/0.75	1.12/2/0.81	<b>1.07/1/0.91</b>
20161021	0.89/1/0.89	1.08/1/0.83	<b>1.05/1/0.89</b>	1.10/2/0.91
20180606	0.84/4/0.78	1.20/3/0.68	1.13/4/0.72	<b>0.97/2/0.84</b>



20180830	<b>0.97/2/0.83</b>	1.05/2/0.75	1.06/1/0.82	1.05/2/0.81
20180916	0.80/3/0.86	1.05/2/0.62	0.95/3/0.81	<b>0.97/1/0.85</b>
Average	0.95/2.1/0.80	1.08/2.8/0.70	1.07/2.3/0.76	<b>1.02/1.4/0.87</b>

502 **Table 7.** Comparison of four routing methods for the Longhu River basin

Event number	$(Q_p^s / Q_p^o) / ( t_p^s - t_p^o ) / (E_{NS})$			
	SUH	DUH	TDUH	Proposed
20030517	1.11/4/0.96	1.14/2/0.87	1.00/1/0.88	<b>1.00/2/0.97</b>
20060601	0.92/2/0.83	1.06/1/0.92	<b>1.00/1/0.96</b>	0.95/1/0.88
20060808	1.12/1/0.81	1.23/2/0.85	1.10/2/0.85	1.03/1/0.93
20120527	<b>0.96/0/0.98</b>	1.06/2/0.73	0.94/2/0.78	0.99/1/0.93
20130713	0.85/0/0.95	1.07/1/0.88	0.95/0/0.90	<b>0.91/0/0.94</b>
20161021	0.87/2/0.89	1.18/3/0.88	1.03/3/0.91	<b>1.06/1/0.94</b>





506 **Figure 11.** Comparison of flow hydrographs obtained by the four methods. (a) Flow  
507 event No.20130720. (b) Flow event No.20130817. (c) Flow event No.20150709. (d)  
508 Flow event No.20160128. (e) Flow event No.20161021. (f) Flow event No.20180916.

509 For the flow event No.20161021, the simulation result of the proposed method  
510 was basically consistent with that of the TDUH method. This was because the  
511 antecedent rainfall was close to saturation under this flow event. As a result, the  
512 proposed method performed the same as the TDUH method when the watershed was  
513 saturated. For the flow event No.20180916, the simulation accuracy of the proposed  
514 method was lower than that of the TDUH. The possible reason for the inaccurate flow  
515 simulation is that the antecedent rainfall was relatively small. Because the runoff  
516 generation was not dominated by the saturation-excess, and it was not appropriate to  
517 calculate runoff with the XAJ model.

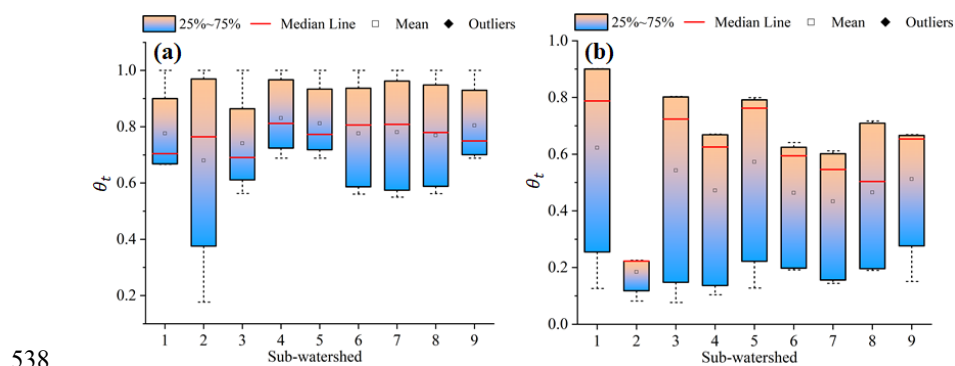
#### 518 *5.4 Influence of time-varying soil moisture content on flow forecasts*

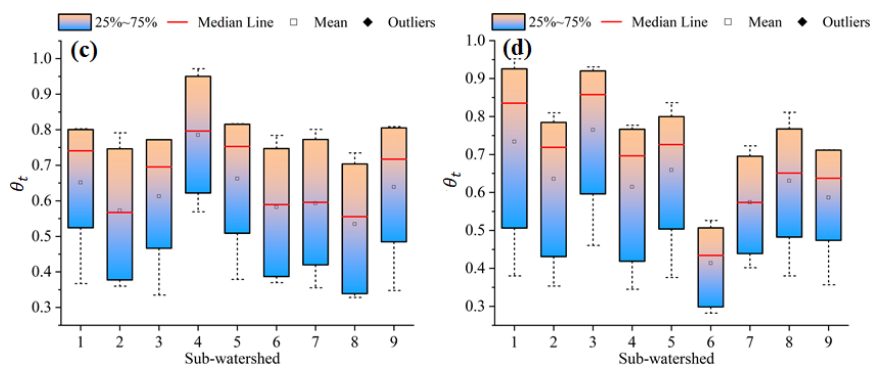
519 In order to evaluate the influence of time-varying soil moisture content on flow  
520 forecasts, three typical flow forecasting results of the proposed method were selected  
521 for comparison in the Qin River basin. Specifically, compared with the forecasting  
522 results using TDUH, the results of the flow event No.20130817 using the proposed  
523 method were relatively similar, the results of the flow events No.20150709 and  
524 20160128 had a better performance, and the results of the flow event No.20180916  
525 were poor. Their corresponding temporal evolution of soil moisture content in  
526 unsaturated regions were obtained. The box-and-whisker plots of soil moisture contents





527 of all sub-basins for flow events No.20130817, 20150709, 20160128 and 20180916 are  
528 shown in Fig. 12. It can be seen from Fig. 12 that the soil moisture content of each sub-  
529 basin was initially low, then the soil moisture content of the sub-basin gradually  
530 increased. Meanwhile, it was obvious that  $\theta_t$  was hard to reach the maximum value.  
531 For all flow events, 9 sub-basins eventually reached the saturation only under the  
532 condition of flow event No.20130817. The mean values of  $\theta_t$  for flow events  
533 No.20150709, 20160128 and 20180916 ranged from 0.5 to 0.8, and the soil moisture  
534 content did not reach the maximum during the flow events. As shown from the observed  
535 flow in Fig. 10, the peak discharge of the flow event No.20130817 was larger than those  
536 of other flow events, reaching 3500 m<sup>3</sup> /s, which meant that the watershed more  
537 probably reached saturation during the flow period.





539

540 **Figure 12.** Distributions of time-varying  $\theta_t$  at different times in each sub-basin using  
541 the proposed TDUH method. (a) Flow event No.20130817. (b) Flow event  
542 No.20150709. (c) Flow event No.20160128. (d) Flow event No.20180916.  $\theta_t$   
543 represents the ratio of current soil moisture storage to the corresponding maximum soil  
544 moisture capacity in the unsaturated region.

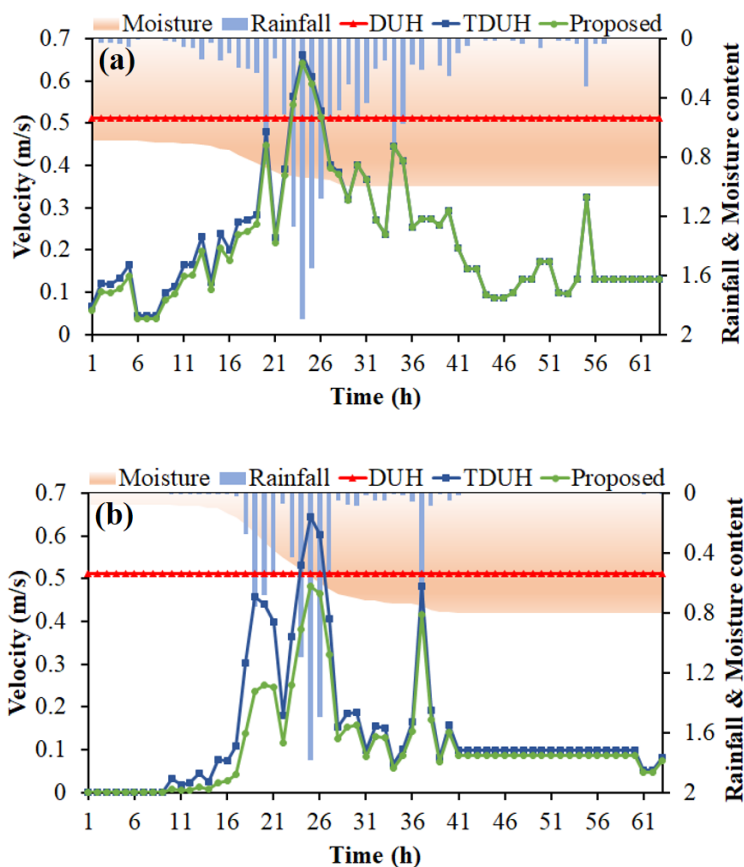
545 As discussed in Section 5.3, the results of the flow event No.20130817 using the  
546 proposed routing method showed the same behavior as did TDUH. This was because  
547 the simulation performance of the proposed method considering time-varying soil  
548 moisture content was the same as that of TDUH when the soil moisture content was  
549 closer to 1. Additionally, the forecast results of the flow events No.20150709, 20160128  
550 with the proposed routing method were obviously better than those of DUH and TDUH.  
551 The reason can be summarized as follows. The mean values of  $\theta_t$  ranged from 0.5 to  
552 0.6 for the two flow events and the  $\theta_t$  values were initially low as shown in Fig. 12.  
553 Thus, the soil moisture content had a significant impact on the shape of the hydrograph.  
554 For the flow event No.20180916, the sub-basins did not reach a global saturation, and  
555 the time-varying values of  $\theta_t$  were generally high, which led to lower flow velocity



556 than in the TDUH method. The peak occurrence times of unit hydrographs used for  
557 runoff routing calculations were general later, leading to a lag time between maximum  
558 rainfall intensity and peak discharge for the forecasting result of the flow event  
559 No.20180916.

### 560 *5.5 Comparison of velocity calculated by three DUH methods*

561 The routing method considering both time-varying rainfall intensity and soil  
562 moisture content was more accurate as discussed in Section 5.3. To evaluate the effect  
563 of time-varying soil moisture content on flow velocity, we selected a grid cell in sub-  
564 basin 3, in which slope and land type parameters were constant. Then, the flow velocity  
565 was calculated under different storm conditions. The storm events No.20130817 and  
566 20150709 were selected and compared, because storm event No.20130817 had a high  
567 intensity and long duration, and storm event No. 20150709 had a short period of heavy  
568 rainfall. Thus, soil moisture contents during the two storm events were significantly  
569 different. Fig. 13 shows the time-varying velocity values of a grid cell for storm events  
570 No.20130817 and 20150709. For the two storm events, the mean velocity of the DUH  
571 method was the largest among the three methods, followed by the TDUH method. The  
572 velocity calculated by the proposed method considering soil moisture content was the  
573 smallest. The velocity of DUH method was constant in the two storms, and that of the  
574 TDUH method varied with the change of the excess rainfall. Meanwhile, the flow  
575 velocity of the proposed method was not only dominated by rainfall intensity, but also  
576 related to soil water content.



577

578

579 **Figure 13.** Time-varying velocity values of a grid cell in different storm events. (a)  
 580 Time-varying velocity in storm event No.20130817. (b) Time-varying velocity in storm  
 581 event No.20150709. The rainfall content is  $I_s$ , and the soil moisture content is  $\theta_s$ .

582 For the storm event No.20130817, the initial soil moisture content was large, and  
 583 it reached the maximum rapidly. The flow velocity of the proposed method was slightly  
 584 smaller than that of the TDUH method at the initial stage of storm events. When the  
 585 whole basin reached saturation, the flow velocities of the two methods became equal.  
 586 Therefore, the differences between hydrographs were small when using the TDUH



587 method and the proposed method for flow routing calculation, which led to similar  
588 forecast results.

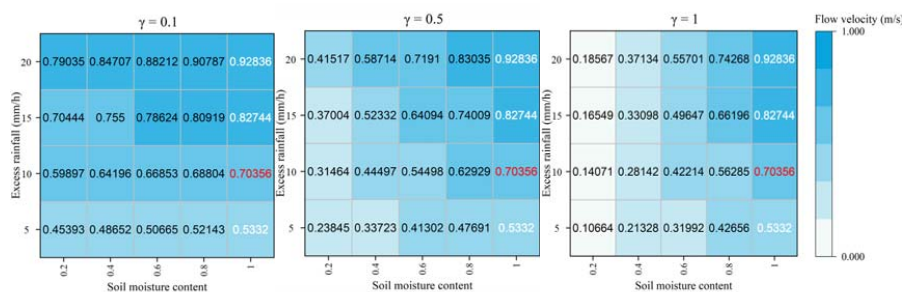
589 For storm event No.20150709, the initial soil moisture content was small, and the  
590 entire basin could not reach the saturation after the rainstorm. Therefore, the grid  
591 velocity in the early stage of the storm was greatly affected by the soil moisture content.  
592 In the later stage of the rainstorm,  $\theta_t$  of the watershed did not reach the maximum,  
593 and was nearly close to 1. Thus, the impact of later soil moisture content on the flow  
594 velocity was small. From the above analyses, it can be concluded that the shape and  
595 duration of the unit hydrograph were mainly related to the soil moisture content at the  
596 initial stage of a storm, and when the watershed was approximately saturated, the grid  
597 flow velocity was mainly dominated by the excess rainfall.

### 598 *5.6 Sensitivity analysis for the proposed TDUH method*

599 A sensitivity analysis for the proposed formula was conducted in the Longhu River  
600 basin. The improved method is only with two additional parameters, compared with the  
601 current model. The objective of this study is to explore the influence soil moisture  
602 content factor on the performance of the DUH model. The parameter  $\gamma$  in Eq. (3)  
603 mainly affected the significant degree of influence over how large that soil moisture  
604 content will be. Thus, sensitivity analysis for parameter  $\gamma$  was necessary. A specific  
605 grid cell in the Longhu River basin was taken as an example, where the slope of the  
606 grid cell was set to 0.22 m/m. The coefficient of flow velocity  $k$  and the ratio of rainfall  
607 intensity to the reference rainfall intensity  $I_s$  were assumed to be 1.5 m/s and 1,



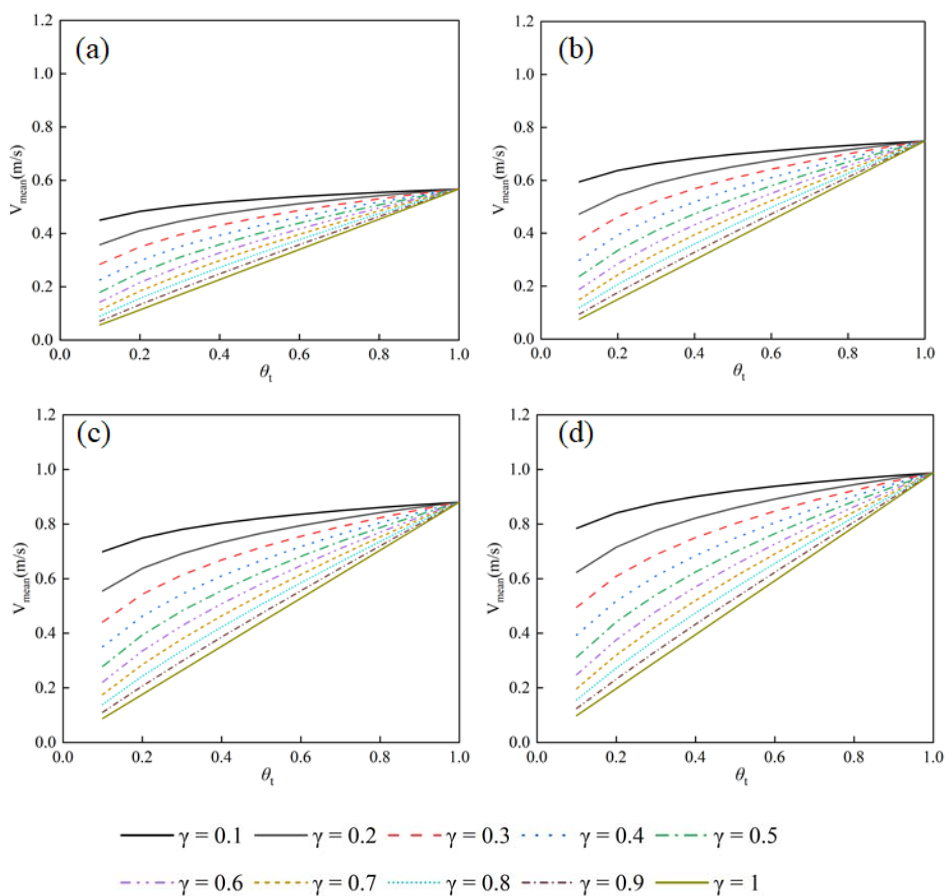
608 respectively. When parameter  $\gamma$  was 0.1, 0.5 and 1, respectively, the hillslope flow  
 609 velocity values corresponding to different rainfall and soil moisture contents using the  
 610 proposed formula are given in Fig. 14.



611  
 612 **Figure 14.** Time-varying flow velocity values corresponding to different parameters

613 It can be seen from Fig. 14 that when  $\theta_t$  was equal to 1, the proposed Eq. (3)  
 614 turned to Eq. (2). The flow velocity values in the last column were the same and only  
 615 changed with rainfall intensities. When  $I_t$  was equal to the reference rainfall  $I_c$ , Eq. (2)  
 616 turned to Eq. (1), and the flow velocity was 0.704 m/s. After introducing a soil moisture  
 617 content factor into the flow velocity formula, the flow velocity values ranged from  
 618 0.107 m/s to 0.928 m/s when  $\gamma$  was equal to 1. The flow velocity values were  
 619 significantly different corresponding to different values of parameter  $\gamma$ . Thus, the  
 620 parameter  $\gamma$  significantly affected the performance of the new routing method.

621 Moreover, the mean flow velocity of the Longhu River basin was calculated under  
 622 different rainfall intensities (e.g.  $\frac{I_t}{I_c} = 0.5, 1, 1.5, 2$ , respectively). Fig. 15 plots the  
 623 theoretical curve of mean velocity and soil moisture content.



624

625

626 **Figure 15.** The theoretical curve of mean velocity and soil moisture content for the

627 Longhu River basin. (a)  $\frac{I_l}{I_c} = 0.5$ . (b)  $\frac{I_l}{I_c} = 1$ . (c)  $\frac{I_l}{I_c} = 1.5$ . (d)  $\frac{I_l}{I_c} = 2$ .

628 Fig. 15 shows that the mean flow velocity ranged from 0.6 to 1 under different  
 629 rainfall intensities without considering the influence of soil moisture content. After  
 630 introducing this new factor into the current flow velocity formula, the mean flow  
 631 velocity was significantly influenced by the exponent  $\gamma$ . In addition, when the soil  
 632 moisture content exceeded 0.7, the variation range of mean flow velocity decreased  
 633 sharply. Results showed that the influence of parameter  $\gamma$  on the flow velocity



634 decreased gradually with the increase of soil moisture content.

## 635 **5. Conclusions**

636 An improved distributed unit hydrograph method considering time-varying soil  
637 moisture content was proposed for flow routing. The proposed method  
638 comprehensively considered the changes of time-varying soil moisture content and  
639 rainfall intensity. The response of the underlying surface to the soil moisture content  
640 was considered as an important factor. The Qin River basin and Longhu River basin  
641 were selected as two case studies. The SUH, DUH, TDUH and proposed routing  
642 methods were used for flow forecasting, and simulated results were compared. The  
643 sensitivity analysis was conducted for parameter  $\gamma$ . The main conclusions can be  
644 summarized as follows.

645 (1) The proposed runoff routing method, considering both time-varying rainfall  
646 intensity and soil moisture content, was proposed, and the influence of the  
647 inhomogeneity of runoff generation on the routing process was considered. It was found  
648 that the soil moisture content was a significant factor affecting the accuracy of flow  
649 forecasts, especially in the catchment dominated by saturation-excess runoff, and the  
650 flow velocity increased gradually with more surface runoff after considering the soil  
651 moisture content in unsaturated regions.

652 (2) The time-varying characteristics of the DUH can be further considered by  
653 introducing both rainfall intensity and soil moisture content into the flow velocity





654 formula, which can effectively improve the accuracy of flow forecasts. Simulation  
655 hydrographs and criteria of the two case studies showed that the accuracy of the  
656 proposed method was the highest, followed by the SUH and TDUH methods, and  
657 finally the DUH method.

658 (3) The shape and duration of the improved TDUH considering soil moisture were  
659 mainly affected by rainfall intensity. Meanwhile, soil moisture content at initial stage  
660 of a storm also played a significant role in the characteristics of the improved TDUH.  
661 When the watershed is approximately saturated, the grid flow velocity was mainly  
662 dominated by excess rainfall.

663 (4) Results of sensitivity analysis showed that the accuracy of the proposed method  
664 was mainly affected by soil moisture content. The influence of parameter  $\gamma$  on the  
665 flow velocity decreased gradually with the increase of soil moisture content.

#### 666 **Data availability**

667 Due to the strict security requirements from the departments, some or all data, models,  
668 or code generated or used in the study are proprietary or confidential in nature and may  
669 only be provided with restrictions (e.g. anonymized data).

#### 670 **Author contributions**

671 Lu Chen conceived the original idea, and Bin Yi designed the methodology. Ping Jiang  
672 collected the data. Bin Yi developed the code and performed the study. Bin Yi, Lu Chen,  
673 Hansong Zhang and Vijay P. Singh contributed to the interpretation of the results. Bin



674 Yi wrote the paper, and Lu Chen, Vijay P. Singh revised the paper.

#### 675 **Competing interests**

676 The authors declare that they have no conflict of interest.

#### 677 **Acknowledgments**

678 This research has been supported by the National Outstanding Youth Science Fund

679 Project of National Natural Science Foundation of China (No. 51922047), and the

680 General Program of National Natural Science Foundation of China (No. 51879109).

#### 681 **References**

682 Anderson, AE, Weiler, et al., Hudson Subsurface flow velocities in a hillslope with  
683 lateral preferential flow. *Water Resources Research*, 45, pp. W11407,  
684 <https://doi.org/10.1029/2008WR007121>, 2009.

685 Alfieri, L., Burek, P., Feyen, L. and Forzieri, G.: Global warming increases the  
686 frequency of river floods in Europe. *Hydrology and Earth System Sciences*.  
687 19:2247-2260, <https://doi.org/10.5194/hess-19-2247-2015>, 2015.

688 Bhunya, P. K., Ghosh, N. C., Mishra, S. K., Ojha, C. S. and Berndtsson, R.: Hybrid  
689 Model for Derivation of Synthetic Unit Hydrograph. *Journal of Hydrologic  
690 Engineering*, 10(6):458-467, [https://doi.org/10.1061/\(ASCE\)1084-  
0699\(2005\)10:6\(458\)](https://doi.org/10.1061/(ASCE)1084-<br/>691 0699(2005)10:6(458)), 2005.

692 Beskow, S., Mello, C. R., Norton, L. D. and da Silva, A. M.: Performance of a  
693 distributed semi-conceptual hydrological model under tropical watershed  
694 conditions. *Catena*, 86(3):160-171, <https://doi.org/10.1016/j.catena.2011.03.010>,  
695 2011.

696 Bhattacharya, A. K., McEnroe, B. M., Zhao, H., Kumar, D., and Shinde, C.: Modclark  
697 model: improvement and application. *Journal of Engineering*, 2(7):100-118,  
698 <https://doi.org/10.9790/3021-0271100118>, 2012.

699 Brenden, J., Stefan H. S., Luc, F., Jeroen, C. J. H. Aerts, Reinhard, M., Wouter Botzen,  
700 W. J., Laurens M. B., Georg, P., Rodrigo, R. and Philip, J. W.: Increasing stress on  
701 disaster-risk finance due to large floods. *Nature Climate Change*, 4(4):264-268,  
702 <https://doi.org/10.1038/nclimate2124>, 2014.

703 Bhuyan, M. K., Kumar, S., Jena, J. and Bhunya, P. K.: Flood Hydrograph with Synthetic  
704 Unit Hydrograph Routing. *Water Resources Management*, 29(15):5765-5782,



- 705 <https://doi.org/10.1007/s11269-015-1145-1>, 2015.
- 706 Bunster, T., Gironás, J., Niemann, J. D.: On the Influence of Upstream Flow  
707 Contributions on the Basin Response Function for Hydrograph Prediction. *Water*  
708 *Resources Research*, 55 (6), 4915-4935, <https://doi.org/10.1029/2018WR024510>,  
709 2019.
- 710 Brunner M. I., Swain D. L., Wood R. R., Willkofer F., Done J. M., Gilleland E., Ludwig  
711 R. An extremeness threshold determines the regional response of floods to changes  
712 in rainfall extremes. *Communications Earth & Environment*, 2(1),  
713 <https://doi.org/10.1038/s43247-021-00248-x>, 2021.
- 714 Clark, C. O.: Storage and the unit hydrograph. *Transactions*, 69(9):1333-1360,  
715 <https://doi.org/10.1061/TACEAT.0005800>, 1945.
- 716 Chow, V. T.: Handbook of applied hydrology. *Hydrological Sciences Journal*, 10(1),  
717 1964.
- 718 Chow, V. T., Maidment, D. R., and Mays, L. W. *Applied hydrology*, McGraw-Hill, New  
719 York, 1988.
- 720 Chinh, L., Iseri, H., Hiramatsu, K., Harada, M. and Mori, M.: Simulation of rainfall  
721 runoff and pollutant load for Chikugo River basin in Japan using a GIS-based  
722 distributed parameter model. *Paddy and Water Environment*, 11(1-4):97-112,  
723 <https://doi.org/10.1007/s10333-011-0296-9>, 2013.
- 724 Dooge, J.: A General Theory of the Unit Hydrograph. *Journal of Geophysical Research*  
725 *Atmospheres*, 64(2):241-256, <https://doi.org/10.1029/JZ064i002p00241>, 1959.
- 726 Duan, Q. Y., Sorooshian, S., Gupta, V.: Effective and efficient global optimization for  
727 conceptual rainfall-runoff models. *Water Resources Research*. 28(4):1015-1031,  
728 <https://doi.org/10.1029/91WR02985>, 1992.
- 729 Du, J., Xie, H., Hu, Y., Xu, Y. P. and Xu, C. Y.: Development and testing of a new storm  
730 runoff routing approach based on time variant spatially distributed travel time  
731 method. *Journal of Hydrology*, 369(1-2):44-54,  
732 <https://doi.org/10.1016/j.jhydrol.2009.02.033>, 2009.
- 733 Gupta, V. K., Waymire, E., Wang, C. T.: A representation of an instantaneous unit  
734 hydrograph from geomorphology. *Water Resources Research*, 16(5): 855-862,  
735 <https://doi.org/10.1029/WR016i005p00855>, 1980.
- 736 Gupta, H. V., Kling, H., Yilmaz, K. K. & Martinez, G. F. Decomposition of the mean  
737 squared error and NSE performance criteria: Implications for improving  
738 hydrological modelling. *Journal of Hydrology*. 377, 80-91,  
739 <https://doi.org/10.1016/j.jhydrol.2009.08.003>, 2009.
- 740 Gironás, J., Niemann, J. D., Roesner, L. A., Rodriguez, F. and Andrieu, H.: A morpho-  
741 climatic instantaneous unit hydrograph model for urban catchments based on the  
742 kinematic wave approximation. *Journal of Hydrology*, 377(3-4),  
743 <https://doi.org/10.1016/j.jhydrol.2009.08.030> 317–334, 2009.
- 744 Gibbs, M. S., Dandy, G. C., Maier, H. R.: Evaluation of parameter setting for two GIS  
745 based unit hydrograph models. *Journal of Hydrology*, 393(3-4), 197–205,  
746 <https://doi.org/10.1016/j.jhydrol.2010.08.014>, 2010.



- 747 Grimaldi, S., Petroselli, A., Alonso, G., Nardi, F. Flow time estimation with spatially  
748 variable hillslope velocity in ungauged basins. *Advances in Water Resources*, 33  
749 (10), 1216-1223, <https://doi.org/10.1016/j.advwatres.2010.06.003>, 2010.
- 750 Grimaldi, S., Petroselli, A., Nardi, F. A parsimonious geomorphological unit  
751 hydrograph for rainfall-runoff modelling in small ungauged basins. *Hydrological*  
752 *Sciences Journal*, 57 (1), 73-83, <https://doi.org/10.1080/02626667.2011.636045>,  
753 2012.
- 754 Gad, M. A.: Flow Velocity and Travel Time Determination on Grid Basis Using  
755 Spatially Varied Hydraulic Radius. *Journal of Environmental Informatics*,  
756 <https://doi.org/10.3808/jei.201400259>, 23(2):36-46, 2014.
- 757 Haan, C.T., Barfield, B.J., Hays J.C.: Design hydrology and sedimentology for small  
758 catchments Academic Press, New York, 1994.
- 759 Hutchinson, D. G., and R. D. Moore, Throughflow variability on a forested hillslope  
760 underlain by compacted glacial till, *Hydrol. Processes*, 14(10), 1751-1766,  
761 [https://doi.org/10.1002/1099-1085\(200007\)14:10<1751::AID-HYP68>3.0.CO;2-](https://doi.org/10.1002/1099-1085(200007)14:10<1751::AID-HYP68>3.0.CO;2-U)  
762 [U](https://doi.org/10.1002/1099-1085(200007)14:10<1751::AID-HYP68>3.0.CO;2-U), 2000.
- 763 Katz, D. M., Watts, F. J., Burroughs, E. R. Effects of Surface Roughness and Rainfall  
764 Impact on Overland Flow. *Journal of Hydraulic Engineering*, 121(7):546-553,  
765 [https://doi.org/10.1061/\(ASCE\)0733-9429\(1995\)121:7\(546\)](https://doi.org/10.1061/(ASCE)0733-9429(1995)121:7(546)), 1995.
- 766 Kilgore, J. L. Development and evaluation of a GIS - based spatially distributed unit  
767 hydrograph model, (Master's thesis). Blacksburg, VA: Virginia Polytechnic  
768 Institute and State University. <http://hdl.handle.net/10919/35777>, 1997.
- 769 Kumar, R., Chatterjee, C., Singh, R. D., Lohani, A. K. and Kumar, S.: Runoff estimation  
770 for an ungauged catchment using geomorphological instantaneous unit  
771 hydrograph (GIUH) models. *Hydrological Processes*, 21(14):1829-1840,  
772 <https://doi.org/10.1002/hyp.6318>, 2007.
- 773 Khaleghi, S., Monajemi, P., Nia, M. P.: Introducing a new conceptual instantaneous unit  
774 hydrograph model based on a hydraulic approach. *Hydrological Sciences Journal*,  
775 63:13-14, <https://doi.org/10.1080/02626667.2018.1550294>, 2018.
- 776 Kong, F. Z., Guo, L.: A method of deriving time-variant distributed unit hydrograph.  
777 *Advances in Water Science*, 30(04):477-484,  
778 <https://doi.org/10.14042/j.cnki.32.1309.2019.04.003>. 2019. (in chinese)
- 779 Linsley, R. K., Kohler, M. A., Paulhus, J. L. *Applied hydrology*. The McGraw-Hill  
780 Book company, Inc., New York, 1949.
- 781 Lee, K. T., Chen, N. C., Chung, Y. R.: Derivation of variable IUH corresponding to  
782 time-varying rainfall intensity during storms. *International Association of*  
783 *Scientific Hydrology Bulletin*, 53(2):323-337,  
784 <https://doi.org/10.1623/hysj.53.2.323>, 2008.
- 785 Mockus, V.: Use of storm and watershed characteristics in synthetic hydrograph  
786 analysis and application. AGU, Pacific Southwest Region Mtg., Sacramento, Calif,  
787 1957.
- 788 Minshall, N. E.: Predicting storm runoff on small experimental watersheds. *J. Hydraul.*



- 789 Engng ASCE, 86(HY8), 17-38, <https://doi.org/10.1061/JYCEAJ.0000509>, 1960.
- 790 Moore, R. J.: The probability-distributed principle and runoff production at point and  
791 basin scales, *Hydrological Sciences Journal*, 30, 273-297,  
792 <https://doi.org/10.1080/02626668509490989>, 1985.
- 793 Maidment, D. R.: Developing a spatially distributed unit hydrograph by using GIS.  
794 IAHS publication, 181-181, 1993.
- 795 Maidment, D. R., Olivera, F., Calver, A., Eatherall, A. and Fraczek, W.: Unit  
796 hydrograph derived from a spatially distributed velocity field. *Hydrological  
797 Processes*, 10: 831-844, [https://doi.org/10.1002/\(SICI\)1099-  
798 1085\(199606\)10:6<831::AID-HYP374>3.0.CO;2-N](https://doi.org/10.1002/(SICI)1099-1085(199606)10:6<831::AID-HYP374>3.0.CO;2-N), 1996.
- 799 Muzik, I.: A GIS-derived distributed unit hydrograph. *Hydrological Processes*,  
800 10(10):1401-1409, [https://doi.org/10.1002/\(SICI\)1099-  
801 1085\(199610\)10:10<1401::AID-HYP469>3.0.CO;2-3](https://doi.org/10.1002/(SICI)1099-1085(199610)10:10<1401::AID-HYP469>3.0.CO;2-3), 1996.
- 802 Martinez, V., Garcia, A. I., Ayuga, F.: Distributed routing techniques developed on GIS  
803 for generating synthetic unit hydrographs. *Transactions of the ASAE*, 45(6):1825-  
804 1834, <https://doi.org/10.13031/2013.11433>, 2002.
- 805 Melesse, A. M., Graham, W. D.: Storm runoff prediction based on a spatially distributed  
806 travel time method utilizing remote sensing and GIS, *Journal of the American  
807 Water Resources Association*, 40 (4), 863-879, [https://doi.org/10.1111/j.1752-  
808 1688.2004.tb01051.x](https://doi.org/10.1111/j.1752-1688.2004.tb01051.x), 2004.
- 809 Munich, R. E.: Natural catastrophe losses at their highest for four years, 2017.
- 810 Mizukami, N., Rakovec, O., Newman, A. J., Clark, M. P., Wood, A. W., Gupta, H. V.,  
811 and Kumar, R.: On the choice of calibration metrics for “high-flow” estimation  
812 using hydrologic models, *Hydrology and Earth System Sciences*, 23, 2601-2614,  
813 <https://doi.org/10.5194/hess-23-2601-2019>, 2019.
- 814 Nash, J. E.: The form of the instantaneous unit hydrograph. *International Association  
815 of Science and Hydrology*, 45(3):114-121, 1957.
- 816 Nash, J. E. & Sutcliffe, I. V. River flow forecasting through conceptual models part I -  
817 a discussion of principles. *Journal of Hydrology*, 10, 282-290,  
818 [https://doi.org/10.1016/0022-1694\(70\)90255-6](https://doi.org/10.1016/0022-1694(70)90255-6), 1970.
- 819 NRCS (natural Resources Conservation Service), Ponds Planning, design, construction.  
820 Washington, DC: US Natural Resources Conservation Service, Agriculture  
821 Handbook no.590, 1997.
- 822 Noto, L. V., Loggia, G. L.: Derivation of a distributed unit hydrograph integrating GIS  
823 and remote sensing. *Journal of Hydrologic Engineering*, 12 (6):639-650,  
824 [https://doi.org/10.1061/\(ASCE\)1084-0699\(2007\)12:6\(639\)](https://doi.org/10.1061/(ASCE)1084-0699(2007)12:6(639)), 2007.
- 825 Nigussie T. A., Yeğen E. B., Melesse A. M.: Performance Evaluation of Synthetic Unit  
826 Hydrograph Methods in Mediterranean Climate. A Case Study at Guvenc Micro-  
827 watershed, Turkey. In: Melesse A., Abteu W. (eds) *Landscape Dynamics, Soils  
828 and Hydrological Processes in Varied Climates*. Springer Geography. Springer,  
829 Cham. [https://doi.org/10.1007/978-3-319-18787-7\\_15](https://doi.org/10.1007/978-3-319-18787-7_15), 2016.
- 830 Peters, D. L., et al. Runoff production in a forested, shallow soil, Canadian Shield Basin,



- 831 Water Resources Research, 31(5), 1291-1304,doi:10.1029/94WR03286, 1995.
- 832 Paul, P. K., Kumari, N., Panigrahi, N., Mishra, A. and Singh, R.: Implementation of  
833 cell-to-cell routing scheme in a large scale conceptual hydrological model  
834 Environmental Modelling & Software, 101(C):23-33,  
835 <https://doi.org/10.1016/j.envsoft.2017.12.003>, 2018.
- 836 Rodríguez-Iturbe, I., Valdes, J. B.: The geomorphologic structure of hydrologic  
837 response. Water Resources Research, 15(6): 1409-1420,  
838 <https://doi.org/10.1029/WR015i006p01409>, 1979.
- 839 Rodríguez-Iturbe, I., González-Sanabria, M., Bras R. L.: A geomorphoclimatic theory  
840 of the instantaneous unit hydrograph. Water Resources Research, 18(4):877-886,  
841 <https://doi.org/10.1029/WR018i004p00877>, 1982.
- 842 Rigon, R., Bancheri, M., Formetta, G. and Lavenne, A.: The geomorphological unit  
843 hydrograph from a historical-critical perspective[J]. Earth Surface Processes &  
844 Landforms, 41(1):27-37, <https://doi.org/10.1002/esp.3855>, 2016.
- 845 Sherman, L. K.: Streamflow from rainfall by the unit-graph method. Engineering News  
846 Record, 108:501-505, 1932.
- 847 Snyder, F. F.: Synthetic unit-graphs. Transactions American Geophysical Union, 19,  
848 447-454, <https://doi.org/10.1029/TR019i001p00447>, 1938.
- 849 Steenhuis, T. S., et al. Preferential flow influences on drainage of shallow sloping soils,  
850 Agric. Water Manage., 14(1-4), 137-151, [https://doi.org/10.1016/0378-3774\(88\)90069-8](https://doi.org/10.1016/0378-3774(88)90069-8), 1988.
- 852 Saghafian, B., Julien, P. Y.: Time to equilibrium for spatially variable watersheds.  
853 Journal of Hydrology, 172 (1-4):231-245, [https://doi.org/10.1016/0022-1694\(95\)02692-I](https://doi.org/10.1016/0022-1694(95)02692-I), 1995.
- 855 Sidle, R. C., et al. Stormflow generation in steep forested head-waters: A linked  
856 hydrogeomorphic paradigm, Hydrological Processes, 14(3), 369-385,  
857 [https://doi.org/10.1002/\(SICI\)1099-1085\(20000228\)14:3<369::AID-HYP943>3.0.CO;2-P](https://doi.org/10.1002/(SICI)1099-1085(20000228)14:3<369::AID-HYP943>3.0.CO;2-P), 2000.
- 859 Sidle, R. C., et al. A conceptual model of preferential flow systems in forested hillslopes:  
860 Evidence of self-organization, Hydrological Processes, 15(10), 1675-1692,  
861 <https://doi.org/10.1002/hyp.233>, 2001.
- 862 SCS. Design of hydrograph. Washington, DC: US Department of Agriculture, Soil  
863 Conservation Service. 2002.
- 864 Sarangi, A., Madramootoo, C. A., Enright, P. and Prasher, S. O.: Evaluation of three  
865 unit hydrograph models to predict the surface runoff from a Canadian watershed.  
866 Water Resources Management, 21(7):1127-1143, <https://doi.org/10.1007/s11269-006-9072-9>, 2007.
- 868 Singh, P. K., Bhunya, P. K., Mishra, S. K. and Chaube, U. C.: An extended hybrid model  
869 for synthetic unit hydrograph derivation. Journal of Hydrology, 336(3-4):347-360,  
870 <https://doi.org/10.1016/j.jhydrol.2007.01.006>, 2007.
- 871 Singh, P. K., Mishra, S. K. and Jain, M. K.: A review of the synthetic unit hydrograph:  
872 from the empirical UH to advanced geomorphological methods. International



- 873 Association of Scientific Hydrology Bulletin, 59(2):239-261,  
874 <https://doi.org/10.1080/02626667.2013.870664>, 2014.
- 875 Singh, S. K.: Simple Parametric Instantaneous Unit Hydrograph. Journal of Irrigation  
876 & Drainage Engineering, 141(5):04014066.1-04014066.10,  
877 [https://doi.org/10.1061/\(ASCE\)IR.1943-4774.0000830](https://doi.org/10.1061/(ASCE)IR.1943-4774.0000830), 2015.
- 878 Singh, V.P.: Hydrologic Systems: Vol. 1. Rainfall-Runoff Modeling. Prentice Hall,  
879 Englewood Cliffs, New Jersey.
- 880 Tsuboyama, Y., et al. Flow and solute transport through the soilmatrix and macropores  
881 of a hillslope segment, Water Resources Research, 30(4),879-890,  
882 <https://doi.org/10.1029/93WR03245>, 1994.
- 883 Tani, M. Runoff generation processes estimated from hydrological observations on a  
884 steep forested hillslope with a thin soil layer, Journal of Hydrology, 200(1-4), 84-  
885 109, [https://doi.org/10.1016/S0022-1694\(97\)00018-8](https://doi.org/10.1016/S0022-1694(97)00018-8), 1997.
- 886 Vrugt, J. A., Gupta, H. V., Dekker, S. C., Sorooshian, S., Wagenere, T. and Boutenf, W.:  
887 Application of stochastic parameter optimization to the Sacramento Soil Moisture  
888 Accounting model. Journal of Hydrology, 325(1-4), 288-307,  
889 <https://doi.org/10.1016/j.jhydrol.2005.10.041>, 2006.
- 890 Wong, T. S. W. Time of concentration formulae for planes with upstream inflow.  
891 Hydrological Sciences Journal, 40(5), 663-666.  
892 <https://doi.org/10.1080/02626669509491451>, 1995.
- 893 Zhao, R. J., Zuang, Y., Fang, L.: The xinanjiang model. IAHS AISH Publ. 129, 351-  
894 356, 1980.
- 895 Zhao, R. J.: Xinanjiang model applied in China. J. Hydrol. 135(1-4), 371-381,  
896 [https://doi.org/10.1016/0022-1694\(92\)90096-E](https://doi.org/10.1016/0022-1694(92)90096-E), 1992.
- 897 Zhou, Q., Chen, L., Singh, V. P., Zhou, J. Z., Chen, X. H. and Xiong, L. H.: Rainfall-  
898 runoff simulation in Karst dominated areas based on a coupled conceptual  
899 hydrological model. Journal of Hydrology, 573: 524-533,  
900 <https://doi.org/10.1016/j.jhydrol.2019.03.099>, 2019.

901